Impact of age hardening on the corrosion characteristics of dissimilar aluminum alloys welded using an innovative MIG welding approach

Sahil Garg [a,*], Arulpandian Palanisamy [b]

[a] GRD Centre for Materials Research, Department of Physics, PSG College of Technology, Coimbatore- 641004, Tamil Nadu, India

[b] Department of Mechanical Engineering, Sri Shakthi Institute of Engineering and Technology, Coimbatore, Tamil Nadu, India

* Corresponding Author: sahilgarg12@gmail.com

Abstract: An innovative metal transfer technique in MIG welding was utilized to join aluminum-based alloys such as 6061 and 5083. Following welding, the specimens underwent heat treatment to explore their corrosion resistance by modifying their microstructure. Tafel polarization curve analysis was employed to evaluate the corrosion performance of the weld zone. The findings indicated that finer microstructures in the weldment led to a notable shift towards less negative corrosion potentials compared to coarser microstructures observed in the as-welded condition. Scanning electron microscopy and X-ray diffraction were used to investigate the microstructural morphology and phase identification of the weld zone. The findings of these tests revealed a link between microstructure and corrosion behaviours.

1. Introduction

Aluminum and its alloys are renowned for their exceptional strength-to-weight ratio and formability, making them popular choices for aircraft and automobile components. However, their widespread application is hindered by their poor corrosion resistance. To address this limitation, heat treatment of aluminum alloys can be employed to customize their corrosion properties. During heat treatment, precipitation occurs at elevated temperatures, causing precipitates to accumulate at grain boundaries. Consequently, the dissolution of the alloy primarily occurs at these enriched precipitate sites. Therefore, intergranular corrosion (IGC) is heavily influenced by the presence of precipitates at grain boundaries, depleted zones, and alloying segregations.

Studies have indicated that the presence of coarse intermetallic particles affects the corrosion properties of aluminium alloys [1-4]. Grain boundaries are the site of intergranular corrosion (IGC), a type of selective corrosion that is made possible by precipitates that grow there and function as tiny galvanic cells.

Different areas created during welding have varying levels of corrosion resistance in materials that have been welded. [5]. Prior research [6] has indicated that welded zones in most joints are prone to corrosion. Reduced corrosion resistance can be caused by many a reason, such as porosity, fractures, residual stress, poor filler choices, and poor edge design [7]. By fixing these welding flaws, corrosion resistance can be increased. [8].

MIG welding is a popular technique for combining aluminium, however the mechanical qualities of the welds are affected by different metal transfer methods, which affect how successful MIG welding is. The metal transfer mode—the process by which metal droplets separate from the wire electrode and go to the weld pool—is the main factor influencing MIG welding performance. This work investigates a unique method of metal transmission in MIG welding that combines the spray and short circuit modes, made possible by well-chosen process parameters. Superior mechanical qualities were obtained by using this novel approach in comparison to traditional metal transfer strategies. Specifically, the study looks at the impact of ageing time. Heat treatment produces a more homogeneous and finer microstructure, which improves the corrosion resistance of the welds made using the new MIG welding process strategy.

2. Material and Methods

The study employed 6061 and 5083 plates, each with a thickness of 5 mm, which were welded together using ER 5183 filler wire. Table 1 presents a summary of the chemical composition of the parent materials as well as the filler material.

Table 1. Chemical Composition (wt. %) of Aluminum Alloy

Alloy	Al	Mg	Fe	Si	Cu	Zn	Mn	Ti	Cr
AA6061	96.71	1	0.7	0.6	0.25	0.25	0.15	0.15	0.19
AA5083	93.45	4.4	0.4	0.4	0.1	0.25	0.7	0.15	0.15
ER5183	93.1	4.7	0.40	0.40	0.10	0.25	0.75	0.15	0.15

It is inevitable that droplets may occasionally come in touch with one another during such transitions, which can result in a moment of transient short-circuiting, in which the whole

"chain of droplets" makes contact with the molten pool. When this happens, there is usually less spatter activity, especially if re-ignition is not regulated. Consequently, while using a high plasma pressure the amount of heat input in the weld zone is reduced by using a mix of spray and short-circuit modes in conjunction with the welding arc. As a result, the parent material's qualities are not significantly altered.

2.1. Microhardness and heat treatment

To accomplish solution hardening, the samples were heated for eight hours at 530°C in a tube furnace. They were then quenched in water at 40°C. After that, the samples were subjected to precipitation hardening at 200°C for several lengths of time—1 hour, 2 hours, 4 hours, 6 hours, and 8 hours. The samples were taken out of the furnace and allowed to cool naturally by air after the specified times. A Vickers hardness tester (Model-402MVD) was used to assess hardness, and a 100 g load was applied for a 15-second dwell period. At three different distances from the weldment's bottom—two, 2.5, and 3.5 mm—the hardness values were ascertained. Furthermore, tests for hardness were conducted at 0.25 mm intervals from the welding Centre. For corrosion testing, samples with the greatest and lowest microhardness were chosen.

2.2. Corrosion Test

For the corrosion test, the exposed surface area of the samples measured 6 mm x 3 mm, while the remaining portion was coated with a non-conducting material. Age-hardened samples underwent corrosion behavior analysis through potentio-dynamic corrosion testing. Tafel polarization diagrams were generated using Gamry instruments, setting the initial and final potentials relative to the open circuit at -0.25V and 0.25V, respectively, with a scan rate of 0.2 mV/s.

The samples were submerged in an aqueous solution with a pH of 6.8 and 3.5 weight percent NaCl in a corrosion cell. All specimens were mounted, polished, and had their electrical contact restored before testing. To reach cell equilibrium, an open circuit voltage was supplied for sixty minutes. A calomel reference electrode was used in conjunction with two graphite counter electrodes. Additionally, the samples with the greatest and lowest hardness were subjected to scanning electron microscopy (SEM) examination using a JEOL SEM (Model JSM-6610LV) running at 10 kV. The investigation involved the use of a secondary electron detector, and the weld zone was subjected to energy-dispersive X-ray spectroscopy (EDS). Using PANalyticalX'Pert Pro, an X-ray diffraction (XRD) examination of the samples was performed to determine the elements included in the weldment [9]. The generator parameters were 40 mA and 45 kV.

3. Results and Discussion

Figure 1 (a-f) illustrates the microstructure of the weld zone for both sample 1 and sample 2, highlighting both the as-welded and post-weld heat-treated (PWHT) specimens at various heat treatment durations. In Figure 1a, the Chinese script details the morphology of the microstructure, highlighting the emergence of Mg_2Si phase formation. Meanwhile, figure 2b exhibits a finely structured microstructure alongside coarse particles abundant in silicon content.
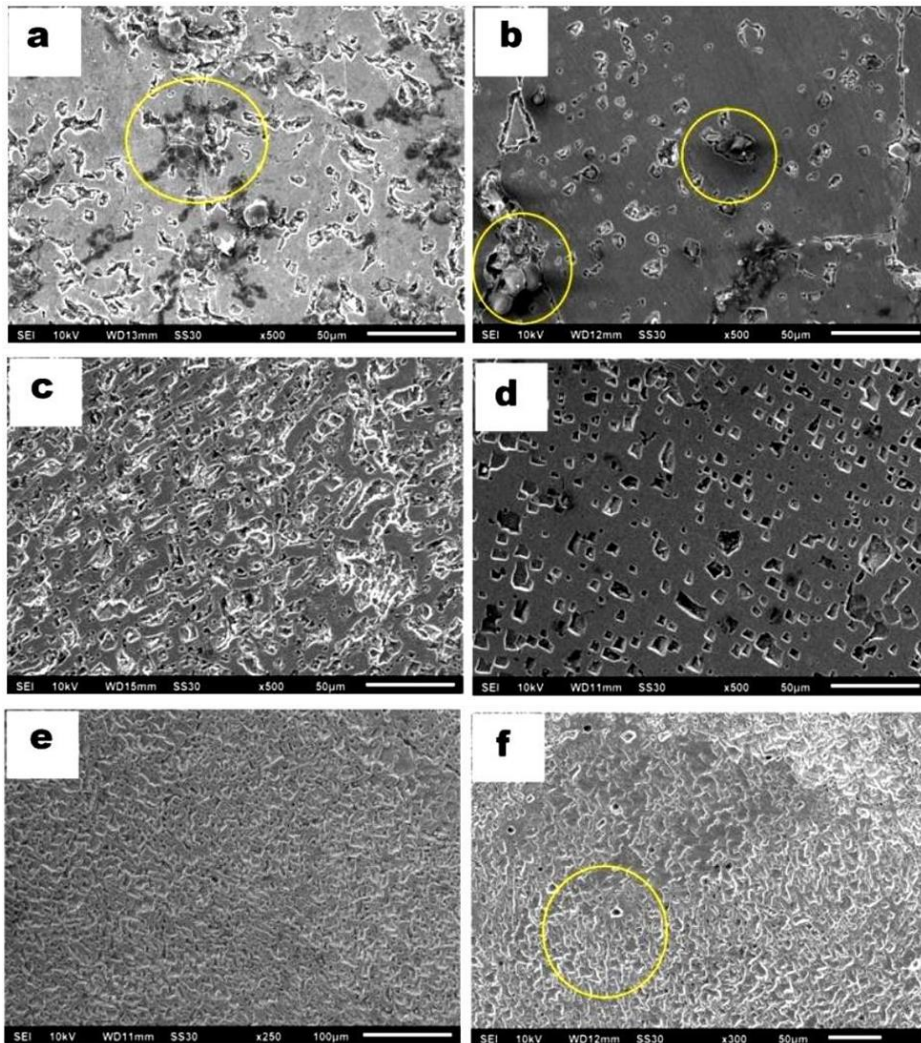
Figure 1. Microstructure of weld zone (a) Sample 1-Aswelded, (b) Sample1- PWHT 3-hour, (c) Sample 1- PWHT 8-hour, (d) Sample 2-Aswelded, (e) Sample2- PWHT 1 hour, (f) Sample 2- PWHT 8 hour

Figure 1c depicts the presence of coarse particles in the weld zone, notable for their high silicon content. In Figure 1d, an irregular distribution of carbon and silicon-based coarse particles is evident. Figure 1e reveals microstructural peaks and valleys with minor porosity, while Figure 1f displays a significant amount of porosity.

Comparison between Figure 1a, Figure 1b, and Figure 1c indicates a decrease in the formation of coarse particles with post-weld heat treatment (PWHT), followed by an increase after a certain duration of heat treatment.

Using a 100 g force, a Vickers microhardness test was performed at three different points on the welded plates: 2.5 mm, 3.5 mm, and 2 mm from the bottom. The average hardness values for various heat treatment durations are shown in Figure 2.

In the as-welded state, Sample 1's maximum reported hardness was around 97.07 HV. Following a four-hour heat treatment following the welding process, the hardness reached 110 HV. Weldment hardness, however, decreased when the heat treatment duration was further extended.

In contrast, Sample 2's as-welded state had the lowest hardness of 40.10 HV. After an hour of heat treatment after the post-weld process, the hardness reached 72.3 HV. Weldment hardness, however, decreased because of further increases in heat treatment duration.

This phenomenon is attributed to the fine and uniform distribution of precipitates at the weld joints achieved through PWHT, combined with the advantageous characteristics of the GMAW method, such as spatter-free welding and low heat input. The improved resistance to crack initiation and propagation contributes to the higher observed hardness values.
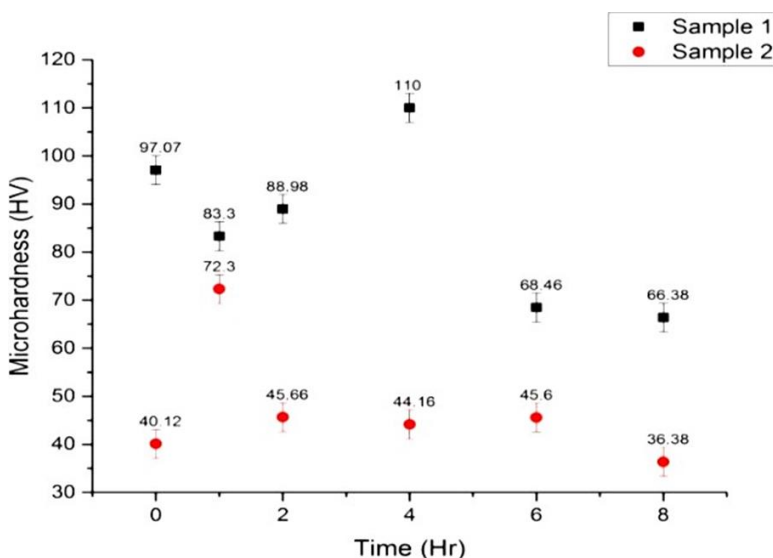
Figure 2. Microhardness data for both as welded and post-weld heat treated (PWHT) joint.

The potentiodynamic polarization curves for the as welded and post-weld heat-treated (PWHT) samples submerged in a 3.5 weight percent NaCl solution are shown in Figure 3. Tafel extrapolation was used to calculate current densities. Based on the enhanced silicon content in the weld zone, Table 2 summarizes the polarization data and shows an increase in corrosion at positive potentials with longer heat treatment durations. Notably, the presence of silicon in a solid solution state enhances aluminum's susceptibility to dissolution at higher potentials.

SEM observations of specimen's post-polarization corrosion test reveal localized pitting corrosion, as illustrated in Fig. 4(a-f). The morphology of the corrosion attack in Fig. 4(a-d) and 4(f) indicates that coarse particles in the intermetallic serve as sites for nucleation and growth. Furthermore, the matrix dislocation initiation is seen in Fig. 4(e). These photos imply that the weld's metal surface is subject to localized attack, and that the corrosion behavior of the weldment is influenced by subsequent phases.

Figures 4(a-f) exhibit surface morphology after exposure to a 3.5 wt. % NaCl solution, where the corrosion potential is directly influenced by the weldment's microstructure. A coarse microstructure in the weldment acts as an active site for corrosion growth and nucleation.

A localized rise in pH in the solution next to the coarse particles results from the potential difference between the particles and the surrounding matrix, which causes matrix disintegration in the surrounding regions.

Table 2. Tafel polarization current density, corrosion potential, and corrosion rate in a 3.5wt% NaCl solution

Sample	Icorr(A)	Ecorr(v)	C.R (mpy)
Sample 1			
As welded	4.65E-06	-0.466	4.459
PWHT-3 Hr	5.65E-07	-0.430	3.031
PWHT-8 Hr	1.04E-06	-0.809	33.025
Sample 2			
As welded	7.95E-07	-0.504	3.412
PWHT-1 Hr	2.45E-07	-0.511	1.502
PWHT-8 Hr	9.46E-07	-0.8	5.071

On the contrary, finer particles tend to develop a protective layer on their surface, thereby diminishing corrosion effects and bolstering the corrosion resistance of the weldments.

Following the polarization corrosion test, XRD analysis was conducted on specimens to investigate the phase composition of the dissimilar aluminum alloy weldment fabricated using the new MIG welding technique. XRD patterns of the welded joints were examined using a copper target, and the results are depicted in Fig. 5(a-f). Parameters relevant to the diffraction peaks in the diagram were determined utilizing X' Pert High Score Plus software.

The study showed that Mg2Si and Mg5Si6 phases made up mostly the weld zone. Due to the abundance of magnesium in the base material and filler wire, silicon (Si) and magnesium (Mg) elements are present. Furthermore, a layer of aluminium oxide was shown to be developed on the Weldment's surface.
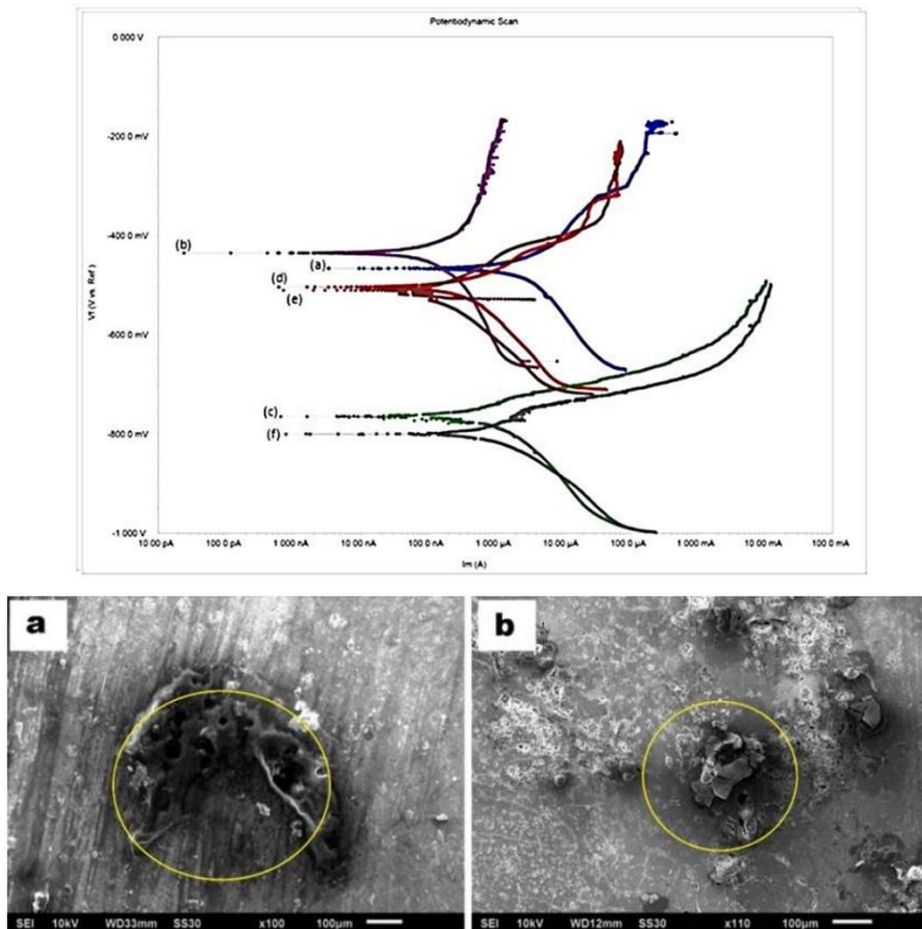
Figure 3. Potentiodynamic polarization curves for Sample 1-Aswelded, Sample 1-PWHT 3 hours, Sample 1-PWHT 8 hours, Sample 2-Aswelded, Sample 2-PWHT 1 hour

Potentiodynamic polarization curves for (a) in Figure 3. Sample 1-Aswelded, Sample 1-PWHT 3 hours, Sample 1-PWHT 8 hours, Sample 2-Aswelded, Sample 2-PWHT 1 hour, and Sample 2-PWHT 8 hours are the samples that are available.
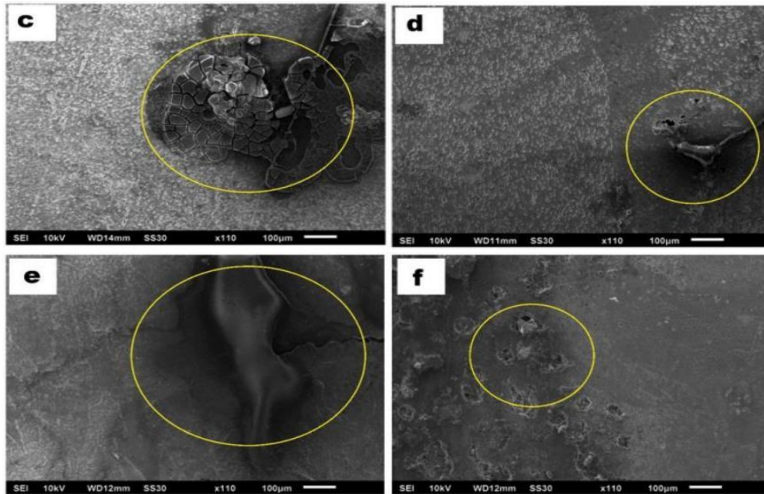
Figure 4. Attack morphology following polarization in the weld (a) Welded, Sample 1 (b) Ex: PWHT for three hours, (c) Ex: PWHT for eight hours, (d) as welded, Sample 2 (e) Sample2: PWHT for one hour, Sample2: PWHT for eight hours
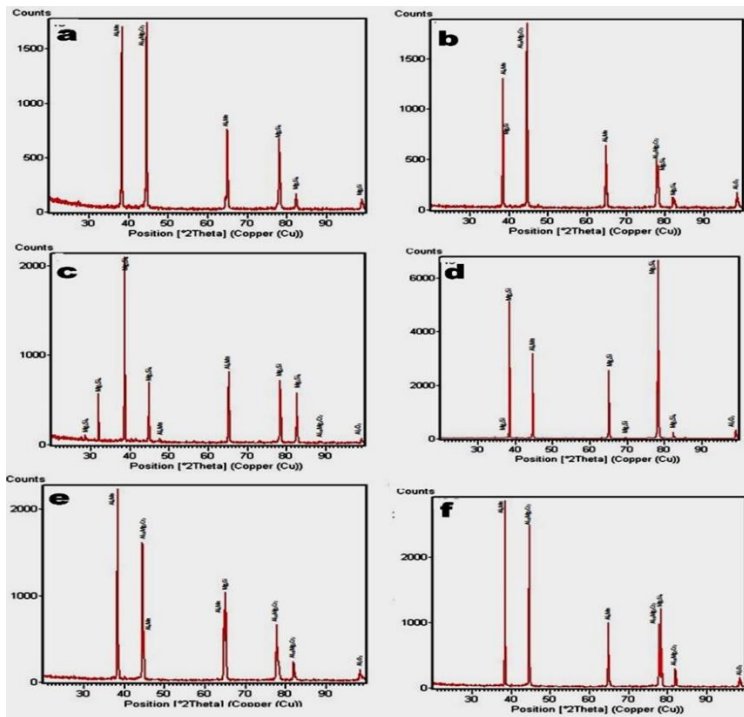
Figure 5. XRD analysis of weld zone after corrosion (a)Sample 1-Aswelded, (b) Sample1-PWHT 3 hr, (c) Sample 1- PWHT 8 hr, (d) Sample 2-As-welded, (e) Sample2- PWHT 1 hr, (f) Sample 2- PWHT 8 hr

5. Conclusion

This study delved into the impact of age hardening on the corrosion behavior of 5 mm thick aluminum 6061 and 5083, employing an innovative MIG welding technique. The shifts in corrosion behavior resulting from microstructural modifications during welding were comprehensively scrutinized using a Tafel polarization cell submerged in a 3.5 wt.% NaCl solution. Based on the investigation, the following conclusions can be inferred:

1. The weld zone exhibited a combination of coarse and fine microstructures, indicating the presence of magnesium (Mg) and silicon (Si) rich particles. These microstructures were attained through post-weld heat treatment (PWHT), facilitated by favorable characteristics of the gas metal arc welding (GMAW) method, such as spatter-free welding and low heat input. Consequently, this led to enhanced resistance against crack initiation and propagation, contributing to the observed high hardness values.

2. Analysis of the potentiodynamic polarization curve revealed an escalation in corrosion at positive potentials with prolonged heat treatment compared to the as-welded condition. This trend can be ascribed to the increased concentration of silicon in the weld zone.

References

[1] R. Ambat, A.J. Davenport, G.M. Scamans, & A. Afseth, Effect of iron-containing intermetallic particles on the corrosion behavior of aluminium, *Corrosion Science*, 48(11), (2006) 3455–3471. https://doi.org/10.1016/j.corsci.2006.01.005

[2] C.M. Liao, R.P. Wei, Galvanic coupling of model alloys to aluminum—a foundation for understanding particle-induced pitting in aluminum alloys, *Electrochimica Acta*, 45(6), (1999) 881-888. https://doi.org/10.1016/S0013-4686(99)00299-6

[3] Z. Szklarska-Smialowska, Pitting corrosion of aluminum, *Corrosion Science*, 41(9), (1999) 1743-1767. https://doi.org/10.1016/S0010-938X(99)00012-8

[4] V. Guillaumin, G. Mankowski, Localized corrosion of 6056 T6 aluminium alloy in chloride media, *Corrosion Science*, 42(1), (2000) 105–125. https://doi.org/10.1016/S0010-938X(99)00053-0

[5] V. Fahimpour, S.K. Sadrnezhaad, F. Karimzadeh, Corrosion behavior of aluminum 6061 alloy joined by friction stir welding and gas tungsten arc welding methods, *Materials and Design*, 39, (2012) 329-333. https://doi.org/10.1016/j.matdes.2012.02.043

[6] D.A. Wadeson, X. Zhou, G.E. Thompson, P. Skeldon, L. Djapic Oosterkamp, G. Scamans, Corrosion behaviour of friction stir welded AA7108 T79 aluminium alloy, Corrosion Science, 48(4), (2006) 887–897. https://doi.org/10.1016/j.corsci.2005.02.020

[7] G. Mathers, (2002) The welding of aluminium and its alloys, *Elsevier Science*.

[8] S. Maggiolino, Ch. Schmid., Corrosion resistance in FSW and in MIG welding techniques of AA6XXX, *Journal of Materials Processing Technology*, 197(1-3), (2008) 237–240. https://doi.org/10.1016/j.jmatprotec.2007.06.034

[9] Y. Yorozu, M. Hirano, K. Oka, Y. Tagawa, Electron spectroscopy studies on magneto-optical media and plastic substrate interface, *IEEE Translation Journal on Magnetics in Japan,* 2(8), (1987) 740–741. https://doi.org/10.1109/TJMJ.1987.4549593